arXiv:1401.7721v1 [cond-mat.mes-hall] 30 Jan 2014

A Gapless MoS_2 Allotrope Possessing Both Massless Dirac and Heavy Fermions

Weifeng Li,[1] Meng Guo,[2] Gang Zhang,[1,*] and Yong-Wei Zhang[1,†]

[1] *Institute of High Performance Computing, A*STAR, Singapore 138632.*

[2] *National Supercomputer Center in Jinan, Jinan, P. R. China 250101.*

(Dated: January 31, 2014)

Abstract

MoS_2, a member of transition metal dichalcogenides (TMDs), recently emerged as one of the fastest growing two-dimensional materials due to its fascinating mechanical, thermal, electronic and optical properties. Unlike graphene which possesses massless Dirac fermions with ultra-high electron mobility, monolayer MoS_2 is a direct band gap semiconductor. An interesting question arises: Can monolayer MoS_2 also possess massless Dirac fermions with ultra-high electron mobility? Here, using first-principles calculations, we show that a monolayer MoS_2 allotrope, which consists of repeated square-octagon rings (abbreviated as so-MoS_2 to distinguish from the normal hexagonal lattice, h-MoS_2) possesses both massless Dirac fermions and heavy fermions. Distinct from the p-orbital Dirac fermions of graphene, the Dirac fermions of so-MoS_2 are d-electrons and possess Fermi velocity comparable to that of graphene. The Dirac cone structure in so-MoS_2 demonstrated here greatly enriches our understanding on the physical properties of TMDs and opens up new possibilities for developing novel electronic/spintronic devices.

INTRODUCTION

One of the exceptional physical properties of graphene is the so-called Dirac cone structure[1]. In the reciprocal space, the valence and conduction bands of graphene, which follow a linear dispersion relation confined to two dimensions, meet at a single point (called Dirac point) at the Fermi level (E_F). This peculiar band structure results in an extremely high charge carrier mobility in the form of massless Dirac fermions, and also many other interesting phenomena, ranging from the formation of conducting edge states in topological insulators to the quantum spin Hall effect due to spin-orbit coupling[1–5]. Since then, a great deal of effort has been made to search for new materials that also possess Dirac cone. Apart from graphene, Dirac cones were also reported in several graphene derivatives[6–9], silicene and hexagonal germanium and their hybrids[2, 10]. Common features of these 2D Dirac systems are: 1) a honeycomb lattice structure; and 2) sp^2 hybridized orbitals near E_F from group IV elements. It is commonly believed that the formation of Dirac cone arises from the strong interplay between electronic and structural properties. For all the known 2D Dirac systems, the three pear-shaped lobes of the sp^2 hybridized orbitals are always in steric compatibility with the honeycomb topology, with no exception.

In recent years, monolayer MoS_2, a member of transition metal dichalcogenides (TMDs), emerged as one of the fastest growing 2D materials[11]. Monolayer MoS_2 shares a similar planar hexagonal lattice to graphene, but its frontier orbitals are dominated by *d*-electrons. In contrast to graphene, monolayer MoS_2 sheet is a semiconductor with no Dirac cone. Although the allotropes of graphene have been studied extensively[6, 7, 12], the allotropes of monolayer MoS_2 have not been explored. Then, a couple of interesting questions arises: Is there any stable allotrope of monolayer MoS_2? If yes, does it possess a Dirac cone electronic structure?

Inspired by recent theoretical and experimental studies of grain boundary atomic structures of monolayer MoS_2[13–15], we first construct a monolayer MoS_2 allotrope with a square crystal lattice. We then reveal that this new monolayer material possesses a nontrivial Dirac cone with massless d electrons. Finally, we perform energetic and phonon spectrum analyses to prove that this novel material is structurally stable. To our best knowledge, this is the first demonstration of Dirac fermions in a monolayer crystal beyond the group IV elements and honeycomb lattice symmetry.

CALCULATION METHODS

All the calculations were performed using Vienna ab-initio simulation package (VASP)[16, 17]. Projector-augmented-wave (PAW) potentials[18] were used to take into account the electron-ion interactions, while the electron exchange-correlation interactions were treated using generalized gradient approximation (GGA)[19] in the scheme of Perdew-Burke-Ernzerhof. A plane wave cutoff of 500 eV was used for all the calculations. All atomic positions and lattice vectors were fully optimized using a conjugate gradient algorithm to obtain the ground-state configuration. A vacuum layer of 25 Å were kept between so-MoS_2 sheets in the $\boldsymbol{c}$ direction to avoid mirror interactions. Atomic relaxation was performed at extremely critical conditions: the change of total energy was less than 0.001 meV and all the Hellmann-Feynman forces on each atom were smaller than 0.0001 eV/Å, which guarantee fully relaxed structures and the accuracy for the following phonon dispersion calculation. A k-point sampling of $7 \times 7 \times 1$ was used for the structure relaxation, while a denser mesh of $45 \times 45 \times 1$ was used to calculate density of states (DOS) and band structures.

The phonon dispersion was calculated using the PHON program[20] based on the finite displacement method. A super-cell containing 3×3 of the primitive-cell was used to calculate the force constant matrix. According to the symmetry operations of $p4$ crystal, there are two in-equivalent atoms in the primitive-cell (one Mo and one S as shown in Fig. 1A and the displacements along the $\boldsymbol{a}$-axis and $\boldsymbol{c}$-axis were considered for each atom (with displacement of 0.04 Å). The forces on all the atoms in the super-cell for each displacement were calculated with VASP with a k-point sampling of $9 \times 9 \times 1$.

RESULTS AND DISCUSSION

In commonly studied monolayer MoS_2, that is, h-MoS_2, the transition metal atoms locate in one sublattice, which is sandwiched by two superimposed chalcogenide atomic layers in the other sublattice. In addition to 6-membered rings, 4- and 8-membered rings consisting entirely of hetero-elemental bonds (S-Mo) were also found at the grain boundaries in monolayer MoS_2[14]. Inspired by these stable grain boundary structures, we construct a monolayer MoS_2 as shown in Fig. 1A by repeating the square-octagon pairs in a square lattice (abbreviated as so-MoS_2 to distinguish from the normal hexagonal lattice, h-MoS_2).

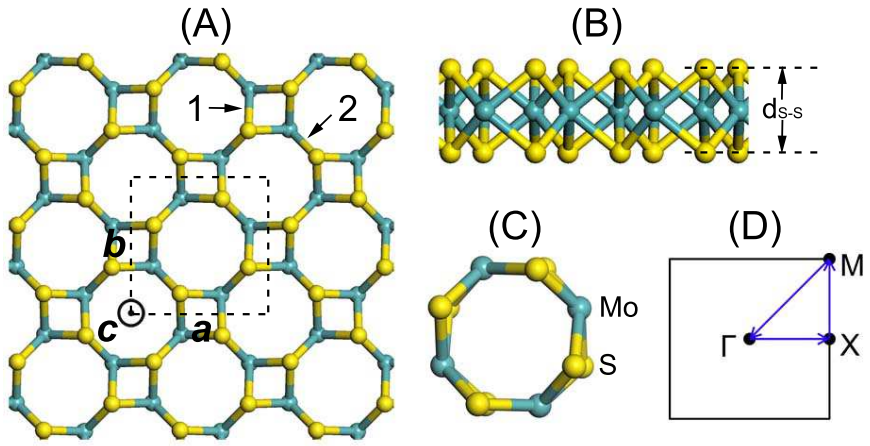

FIG. 1. (A) Top view and (B) side view of so-MoS_2. The dash-line square and bold italic text ***a***, ***b*** and ***c*** in (A) indicate the primitive cell which is also highlighted in (C) and the three lattice vector directions. (D) The first Brillouin zone of so-MoS_2 with letters designating special points and the lines for band structure calculation.

The primitive cell is square with a $p4$ symmetry, containing four Mo and eight S atoms.

The optimized structure of so-MoS_2 has a lattice constant of 6.36 Å. The thickness of the monolayer (measured from S in the top layer to S in the bottom layer as illustrated in Fig. 1B) is 3.12 Å, similar to that of h-MoS_2 which is 3.13 Å. There are structural distortions in so-MoS_2 because of the square-octagon topology: the Mo-S bonds that constitute the square (labelled 1 in Fig. 1A) are stretched to 2.46 Å, while the Mo-S bonds that link the squares (labelled 2 in Fig. 1A) are compressed to a length of 2.39 Å. As a comparison, the Mo-S bond in h-MoS_2 is homogeneously 2.42 Å.

A representative 3D plot that reveals the shape of the conduction and valence bands is shown in Fig. 2A. It is exciting to find that the lower cone (from the valence band) possesses a linear dispersion relation near the Dirac point, indicating massless Dirac fermions. The electronic band structures of so-MoS_2 are shown in Fig. 2B. It is seen that the valence band, conduction band and conduction band+1 (VB, CB and CB+1) approach the Γ point at E_F. The slopes of VB are -16.0 eV·Å(X to Γ) and +15.4 eV·Å(M to Γ), respectively. The upper cone (from CB+1) locates 3 meV above E_F at the Γ point. The slopes of CB+1 branch are +15.6 eV·Å(X to Γ) and -15.5 eV·Å(M to Γ), respectively. We also calculate the Fermi velocity (v_F) of the Dirac fermions using $v_F = \frac{E(k)}{\hbar k}$, which is about 2.3-2.4×10^6 m/s, comparable to that of graphene[9, 21], but an order of magnitude higher than those of

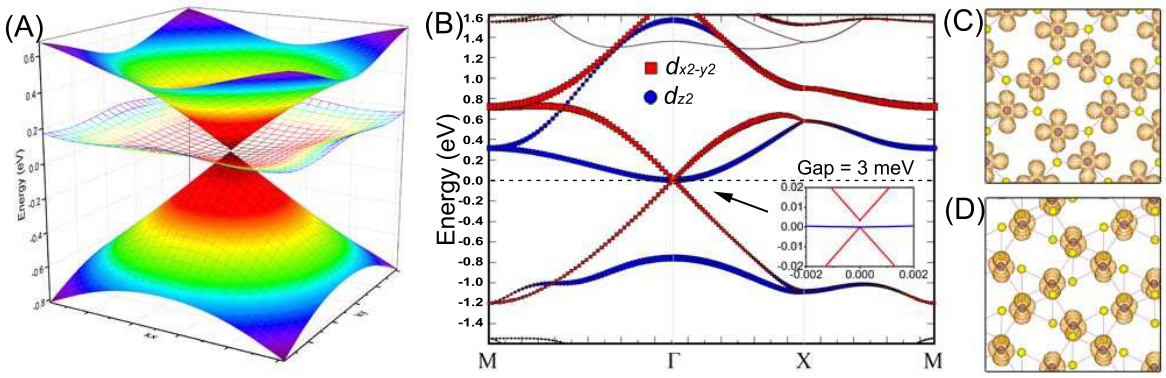

FIG. 2. (A) Dirac cone formed in the vicinity of Dirac point. (B) Electronic band structures of so-MoS_2. (C, D) Charge density plots of the d_{x2-y2} and d_{z2} orbitals of Mo, respectively (electron orbital isosurface level of 0.001 $Å^{-3}$).

hexagonal silicene and germanium monolayer[2, 10]. The CB deviates from the linear slope and is flattened, indicating the coexistence of heavy fermions. The effective mass of these fermions can be estimated using the following equation at the CB minimum.

$$m^* = \frac{\hbar^2}{\partial^2 E(k)/\partial k^2} \tag{1}$$

Our calculations show that the effective masses are 1.11 m_e (X to Γ) and 1.78 m_e (M to Γ), respectively. The complicity of these two un-occupied bands contributes to a moderate level of density of state (DOS) just above E_F, while the DOS just below E_F is zero as shown in Fig. 3A. This implies that, above zero temperature, excitations of electrons to CB and CB+1 are able to cause a high charge carrier density as well as extremely high carrier mobility. Hence a better conductivity than graphene is expected due to its zero carrier density at E_F.

It is well-known that in TMDs, the frontiers orbitals are mainly originated from the *d*-orbitals of transition metals, with weak contribution from the *p*-orbitals of chalcogen atoms[22–26]. In h-MoS_2, d_{xy} and d_{x2-y2} orbitals of Mo are doubly-degenerated in energy, while d_{yz} and d_{xz} are also doubly-degenerated and d_{z2} is singly-denegerated. For S atoms, the p_x and p_y are degenerated. From hexagonal lattice ($p6m$ summatry) to square lattice ($p4$ summatry), some structure symmetries are lost, as well as the electron orbital degeneracies. These changes can be clearly observed from Fig. 3. In so-MoS_2, the VB and CB+1 are mainly described by the d_{x2-y2} orbital of Mo. In the real space, the four pear-shaped lobes

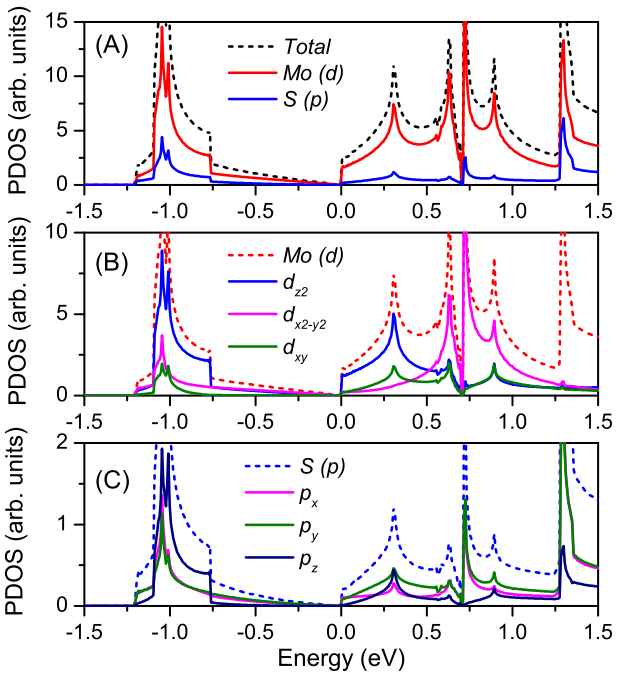

FIG. 3. (A) Total DOS and projections on Mo d- and S p-orbitals; (B) PDOS of Mo d-orbitals and projections on d_{z2}, d_{x2-y2} and d_{xy}; (C) PDOS of S p-orbitals and projections on p_x, p_y and p_z.

of d_{x2-y2} orbital spread in the so-MoS_2 plane and have centres on the $\boldsymbol{a}$ and $\boldsymbol{b}$ lattice axes as shown in Fig. 2C, fully compatible with the square lattice symmetry. Consequently, a long-range coherence is realized between the d_{x2-y2} orbital and the square crystal lattice, leading to the formation of Dirac cone. On the other hand, the CB branch is mainly described by the out-of-plane d_{z2} orbital of Mo. The two pear-shaped regions of d_{z2} are more localized, placing symmetrically on the $\boldsymbol{c}$ axis as shown in Fig. 2D, resulting in the heavy fermions.

In order to assess the stability of the so-MoS_2-based Dirac Fermion system, we first calculated the formation energy (normalized to each atom) defined as:

$$E_{form} = \frac{E_{total} - n_{Mo} \times E_{Mo} - n_S \times E_S}{n_{Mo} + n_S} \tag{2}$$

Our calculation shows that E_{form} is about -4.79 eV/atom, comparable to a value of -5.07 eV/atom for h-MoS_2, indicating that so-MoS_2 is only slightly less stable than h-MoS_2. Furthermore, we also examined the thermal stability by calculating the phonon dispersion relations, which can pinpoint the stability of materials[27]. The phonon band structures are shown in Fig. 4. It is seen that originating from the Γ point, there are three zero-frequency

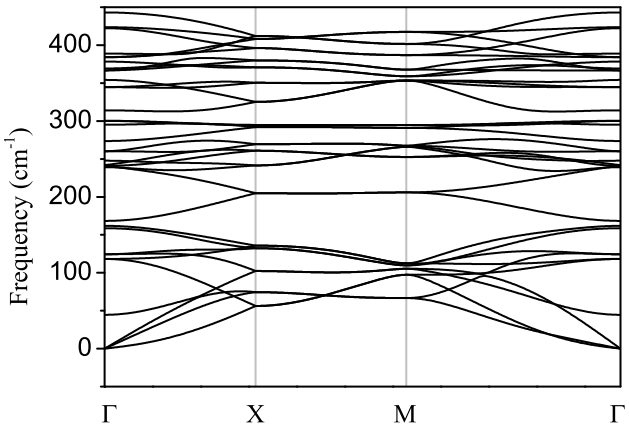

FIG. 4. Phonon band structures of so-MoS_2 along high symmetry directions in the Brillouin zone.

acoustic branches. The lowest branch shows a quadratic energy dispersion relation in k, corresponding to the out-of-plane displacement. The other two branches display a linear k-dependence around the Γ point, representing the in-plane translational and longitudinal displacements in two orthogonal directions. As there are no imaginary frequencies (negative frequencies) found in the phonon spectrum, hence the so-MoS_2 is structurally stable. The possible approach to realize so-MoS_2 is to use novel substrates, like growing hexagonal hafnium (Hf) layer on Ir(111) surface[28] and silicene on Ag(111)[29, 30].

CONCLUSION

To conclude, for the first time, massless Dirac fermions are observed in a member of TMD family, beyond the group IV elements and honeycomb lattice symmetry. We find that the d_{x2-y2} orbitals in so-MoS_2 form a long-range coherence with square lattice structure, leading to the formation of Dirac fermions. We also find that the d_{z2} orbitals locate near E_F, resulting in the coexistence of heavy fermions with massless Dirac fermions in so-MoS_2. Our findings here undoubtedly will not only attract great interest in search for new Dirac fermion materials and their associated new physical properties but also create a world of new possibilities for developing novel electronic, photonic and spintronic atomically-thin layered devices through lattice engineering.

SUPPLEMENTAL MATERIAL

Phonon band structures of so-MoS_2 calculated with the linear response method, and change density plots of the four orbitals near the Fermi level can be found in the Supplemental Material. This material is available at http://XXXXXXX.

This work was supported by the A*STAR Computational Resource Centre through the use of its high performance computing facilities.

---

* zhangg@ihpc.a-star.edu.sg

† zhangyw@ihpc.a-star.edu.sg

[1] A. C. Neto, F. Guinea, N. Peres, K. S. Novoselov, and A. K. Geim, Reviews of modern physics **81**, 109 (2009).

[2] C. C. Liu, W. Feng, and Y. Yao, Physical Review Letters **107**, 076802 (2011).

[3] M. Z. Hasan and C. L. Kane, Reviews of modern physics **82**, 3045 (2010).

[4] X. L. Qi and S. C. Zhang, Physics Today **63**, 33 (2010).

[5] H. Zhang, C.-X. Liu, X.-L. Qi, X. Dai, Z. Fang, and S.-C. Zhang, Nature Physics **5**, 438 (2009).

[6] D. Malko, C. Neiss, F. Vies, and A. Grling, Physical Review Letters **108**, 086804 (2012).

[7] K. K. Gomes, W. Mar, W. Ko, F. Guinea, and H. C. Manoharan, Nature **483**, 306 (2012).

[8] Y. Li, P. Chen, G. Zhou, J. Li, J. Wu, B.-L. Gu, S. Zhang, and W. Duan, Physical Review Letters **109**, 206802 (2012).

[9] C. Hwang, D. A. Siegel, S.-K. Mo, W. Regan, A. Ismach, Y. Zhang, A. Zettl, and A. Lanzara, Scientific Reports **2** (2012).

[10] H. Zhou, M. Zhao, X. Zhang, W. Dong, X. Wang, H. Bu, and A. Wang, Journal of Physics: Condensed Matter **25**, 395501 (2013).

[11] M. Chhowalla, H. S. Shin, G. Eda, L.-J. Li, K. P. Loh, and H. Zhang, Nature Chemistry **5**, 263 (2013).

[12] L. C. Xu, R. Z. Wang, M. S. Miao, X. L. Wei, Y. P. Chen, H. Yan, W. M. Lau, L. M. Liu, and Y. M. Ma, Nanoscale **6**, 1113 (2014).

[13] S. Najmaei, Z. Liu, W. Zhou, X. Zou, G. Shi, S. Lei, B. I. Yakobson, J.-C. Idrobo, P. M. Ajayan, and J. Lou, Nature Materials **12**, 754 (2013).

[14] A. M. van der Zande, P. Y. Huang, D. A. Chenet, T. C. Berkelbach, Y. You, G.-H. Lee, T. F. Heinz, D. R. Reichman, D. A. Muller, and J. C. Hone, Nature Materials **12**, 554 (2013).

[15] Z. Zhang, X. Zou, V. H. Crespi, and B. I. Yakobson, ACS Nano **7**, 10475 (2013).

[16] G. Kresse and J. Furthmuller, Physical Review B **54**, 11169 (1996).

[17] G. Kresse and J. Furthmuller, Computational Materials Science **6**, 15 (1996).

[18] P. E. Blochl, Physical Review B **50**, 17953 (1994).

[19] J. P. Perdew, J. A. Chevary, S. H. Vosko, K. A. Jackson, M. R. Pederson, D. J. Singh, and C. Fiolhais, Physical Review B **46**, 6671 (1992).

[20] D. Alfè, Computer Physics Communications **180**, 2622 (2009).

[21] P. Avouris, Z. Chen, and V. Perebeinos, Nature Nanotechnology **2**, 605 (2007).

[22] A. Kuc, N. Zibouche, and T. Heine, Physical Review B **83**, 245213 (2011).

[23] Y. Ding, Y. Wang, J. Ni, L. Shi, S. Shi, and W. Tang, Physica B: Condensed Matter **406**, 2254 (2011).

[24] D. Voss, P. Krüger, A. Mazur, and J. Pollmann, Physical Review B **60**, 14311 (1999).

[25] K. Albe and A. Klein, Physical Review B **66**, 073413 (2002).

[26] S. W. Han, H. Kwon, S. K. Kim, S. Ryu, W. S. Yun, D. H. Kim, J. H. Hwang, J. S. Kang, J. Baik, H. J. Shin, and S. C. Hong, Physical Review B **84**, 045409 (2011).

[27] H. Peelaers, B. Partoens, and F. Peeters, Nano Letters **9**, 107 (2008).

[28] L. Li, Y. Wang, S. Xie, X.-B. Li, Y.-Q. Wang, R. Wu, H. Sun, S. Zhang, and H.-J. Gao, Nano Letters **13**, 4671 (2013).

[29] B. Feng, Z. Ding, S. Meng, Y. Yao, X. He, P. Cheng, L. Chen, and K. Wu, Nano Letters **12**, 3507 (2012).

[30] P. Vogt, P. De Padova, C. Quaresima, J. Avila, E. Frantzeskakis, M. C. Asensio, A. Resta, B. Ealet, and G. Le Lay, Physical Review Letters **108**, 155501 (2012).